Evolution of high-speed jets and plasmoids downstream of the quasi-perpendicular bow shock

O. Goncharov[1], H. Gunell[1,2], M. Hamrin[1], and S. Chong[1]

[1]Department of Physics, Umeå University, 901 87 Umeå, Sweden.

[2]Royal Belgian Institute of Space Aeronomy, Avenue Circulaire 3, 1180 Brussels, Belgium.

Corresponding author: Oleksandr Goncharov (oleksandr.goncharov@umu.se)

Key Points:

- High-speed jets (plasmoids) downstream of the quasi-perpendicular bow shock are very common.
- The jets grow larger and slower as they move away from the bow shock.
- Jets propagate deeper into the magnetosheath for smaller angles between the interplanetary magnetic field and the bow shock normal.

Abstract

Plasma structures with enhanced dynamic pressure, density or speed are often observed in Earth's magnetosheath. We present a statistical study of these structures, known as jets and fast plasmoids, in the magnetosheath, downstream of both the quasi-perpendicular and quasi-parallel bow shocks. Using measurements from the four Magnetospheric Multiscale (MMS) spacecraft and OMNI solar wind data from 2015–2017, we present observations of jets during different upstream conditions and in the wide range distances from the bow shock. Jets observed downstream of the quasi-parallel bow shock are seen to propagate deeper and faster into the magnetosheath and on towards the magnetopause. We estimate the shape of the structures by treating the leading edge as a shock surface, and the result is that the jets are elongated in the direction of propagation but also that they expand more quickly in the perpendicular direction as they propagate through the magnetosheath.

Plain Language Summary

The solar wind is a stream of charged particles continously emitted from the upper atmosphere of the Sun. When it approaches Earth, it is slowed down and heated to high temperatures in the region called the magnetosheath. However, from time to time plasma jets with speeds close to the solar wind speed are observed in this magnetosheath. They are thought to be formed at the bow shock, which is the boundary between the magnetosheath and the solar wind. In this article, we use data obtained by the four MMS spacecraft, while they passed through the magnetosheath, in a statistical study of the properties of the jets. We have found that they slow down as they move through the magnetosheath and that, in the beginning, they are elongated in the direction of their motion, but also that they expand to become rounder as they move along.

1 Introduction

The bow shock is the first boundary the solar wind encounters as it approaches Earth. Downstream of the shock, in the magnetosheath, the plasma is denser and hotter than in the unperturbed solar wind, and the magnetic field is stronger than the interplanetary magnetic field (IMF). The structure of the bow shock depends to a large extent on whether the IMF is close to parallel or perpendicular to the shock normal. This also affects the particle populations through processes that lead to reflection of particles, the formation of a foreshock and the wave activity in the vicinity of the shock. For small angles between the bow shock normal and the IMF ($\theta_{Bn} < 45^{o}$) the shock is quasi-parallel, and for large angles ($\theta_{Bn} > 45^{o}$) it is known as quasi-perpendicular.

Ions reflected at the quasi-parallel shock travel as beams through the upstream plasma, generating waves in the foreshock region through wave-particle interaction (*e.g. Wilson et al.*, 2013). This is also where Short Large Amplitude Magnetic Structures (SLAMS) have been observed (*Schwartz et al.*, 1992). The quasi-parallel bow shock is replaced repeatedly by newly forming shocks, which leads to strong fluctuations also in the magnetosheath downstream (*Burgess*, 1989; *Schwartz et al.*, 1992; *Scholer and Burgess*, 1992; *Blanco-Cano et al.,* 2006a,b).

During the last two decades, a number of authors have reported observations of plasma entities that stand out from the surrounding magnetosheath by having either an enhanced density, speed or both. A few different terms have been used to denote these

structures, for example, "magnetosheath dynamic pressure enhancements" (*Archer and Horbury*, 2013), "density enhancements" (*Gutynska et al.*, 2015), "transient flux enhancements" (*Němeček et al.*, 1998), "antisunward high-speed jets" (HSJ) (*Plaschke et al.*, 2013), "supermagnetosonic subsolar magnetosheath jets" (*Hietala et al.*, 2012), "high kinetic energy density plasma jets" (*Savin et al.*, 2008), "large-scale jet" (*Dmitriev and Suvorova,* 2015), "super fast plasma streams" (*Savin et al.*, 2012). However, *Gunell et al.,* (2014) used the term "plasmoid" to describe velocity structures with the typical scales on the order of 1 Earth's radii (R_E). The same term was used by *Karlsson et al.,* (2012) to investigate enhancements in the magnetosheath density. In spite of the disparate terminology, on could, in a general sense, treat these terms as synonyms. However, the detailed properties of the entities observed do depend on precise definitions and selection criteria. We shall use the term "jet" for all the plasma entities in our dataset and "fast plasmoid" for the subset whose elements also show a speed increase of 10% or more. The criteria used in this work, and in some of the previously published studies are summarized in Table 1.

Statistical studies have shown that jet occurrence is almost exclusively controlled by the angle between the IMF and the Earth–Sun line (cone angle), while other solar wind parameters or their variability only play a minor role. The jets are predominantly observed when this cone angle is small, that is to say, downstream of the quasi-parallel shock (*Hietala and Plaschke, 2013; Archer and Horbury, 2013; Plaschke et al., 2013*). It was also found that 97% of the observed jets can be formed locally at the bow shock – as opposed to upstream in the solar wind– by ripples that appear on the shock when it is quasi-parallel (*Hietala and Plaschke, 2013)*.

On the other hand, at the flanks of the magnetosheath, the magnetosheath plasma stream is itself super-magnetosonic and bow shock ripples would not necessarily create discernible jets. *Archer and Horbury* (2013) reported that jets become less common toward the flanks. However, *Karlsson et al.,* (2015) observed density enhancements throughout the dayside flanks. Despite the increasing number of observational studies, the jet formation mechanism remains an open question. *Karlsson et al.,* (2015) suggested that SLAMS (*Schwartz,* 1991; Schwartz *et al.*, 1992), could transform into jets when traveling through the bow shock. It was found in a global hybrid-Vlasov simulation that a jet can be created through the interaction between the bow shock and a SLAMS-like structure passing through it (*Palmroth et al.,* 2018). *Wilson et al.,* (2013) studied SLAMS and other structures in the terrestrial foreshock and concluded that groups of SLAMS can act as a local quasi-perpendicular shock.

In contrast to the quasi-parallel bow shock, the quasi-perpendicular shock is well-defined, with a relatively thin ion ramp (thickness of several thermal gyroradii), and the magnetosheath is less turbulent downstream of the quasi-perpendicular than the quasi-parallel bow shock. The reflected ions gain enough energy to pass through the shock front from only one full gyromotion, and there is not enough time for waves to grow. Nevertheless, locally generated waves have been observed in the downstream region (*Mazelle et al.*, 2003; *Lembège et al.*, 2004; *Ofman et al.*, 2009; *Yang et al.*, 2009a, 2009b, 2012; *Ofman and Gedalin*, 2013; *Němeček et al*., 2013; *Goncharov et al.,* 2014; *Soucek et al.*, 2015; *Hoilijoki et al.,* 2016). *Gutynska et al.*, (2015) performed an analysis of the wave properties for understanding the nature of the magnetosheath plasma structures, and concluded that events with significant density and pressure enhancements are fast magnetosonic waves. Global

electromagnetic hybrid simulations (*Omidi et al.,* 2014) suggest that jets that have been formed at the quasi-parallel bow shock for small IMF cone angles may extend into the quasi-perpendicular magnetosheath.

In this paper, we investigate jets in the quasi-perpendicular magnetosheath, their evolution and relation to upstream parameters, and compare with previous statistical studies of jets, downstream of the quasi-parallel bow shock. We use data from the four Magnetospheric Multiscale (MMS) spacecraft (*Burch et al.,* 2016), orbiting in the magnetosheath and bow shock region, and NASA OMNI high resolution solar wind data (*King and Papitashvili,* 2005), gathered during the years 2015–2017. We compare several models of the jet formation mechanism and provide quantitative predictions of jet propagation toward the magnetopause.

Table 1. Summary of the denominations and selection criteria used here and in some of the previously published articles.

Denomination	Criterion	Reference
Dynamic pressure enhancement	At least a 100% increase of P_d above a 20 min running average	Archer & Horbury (2013)
Plasmoid	At least a 100% increase of $\|v_x\|$ above a 10 min average after s/c magnetosheath entry, $v_x<0$	Gunell et al. (2014)
Embedded plasmoid	At least a 50% increase of n_e and less than 10% increase of v above a 500 s running average	Karlsson et al. (2012)
Fast plasmoid	At least a 50% increase of n_e and at least 10% increase of v above a 500 s running average	Karlsson et al. (2012)
Diamagnetic plasmoid	At least a 50% increase of n_e (30% in solar wind) and $\Delta B<0$ (ΔB: maximum deviation from a 5-10 min average before or after plasmoid encounter)	Karlsson et al. (2015)
Paramagnetic plasmoid	At least a 50% (30% in solar wind) increase of n_e and $\Delta B>0$ (ΔB defined as above)	Karlsson et al. (2015)
Anti-sunward high-speed jet	$P_{dx}>0.25\ P_{dsw}$ throughout plasmoid and $\max(P_{dx})> 0.5\ P_{dsw}$	Plaschke et al. (2013)
Jet	$P_{dx}>0.4\ P_{dsw}$ throughout plasmoid and $\max(P_{dx})>P_{dsw}$ and $\max(P_{dx})$ at least twice a 20 min running average	This work
Fast plasmoid	Same as jet condition on P_{dx} in this work and a 10% increase of v above a 20 min running average	This work

2 Dataset and Methodology

From October 2015, the orbits of MMS spacecraft cover a broad region of the magnetosheath. Our visual inspection of the ion energy spectra, plasma and magnetic field signatures in MMS Quicklook plots (https://lasp.colorado.edu/mms/sdc/public/plots/) excluded the magnetosphere and solar wind parts. We used fast survey mode resolution of the magnetic field (16 Hz) and plasma (4.5 s/sample) measurements (*Russell et al.*, 2014;

Pollock et al., 2016). The electric current density, ***J***, was estimated by the curlometer method from the four MMS magnetic field data (*Paschmann and Schwartz,* 2000; *Dunlop et al.*, 2002).

Different physical parameters have been used to identify jets previously. The choice of parameters often affect the nomenclature and the numbers of selected events. The best choice of an identification criterion to use in future studies is still under debate, and it will depend on the particular science questions, and the availability of measurements. In this work, we compared several criteria, which have been adopted from previous observational studies. Each selected interval of the magnetosheath region was automatically analyzed to look for the enhancements in the anti-sunward (negative-x component of the) velocity (*Hietala et al*., 2009, 2012; *Gunell et al.,* 2014). All events were visually inspected and compared with the *Plaschke et al.* (2013) identification criterion, defined by the ratio of the magnetosheath dynamic pressure in the X direction ($P_{dx} = \rho \cdot V_x^2$) to the upstream solar wind dynamic pressure ($P_{dsw} = \rho \cdot V_{sw}^2$), where ρ is the mass density. According to their selected criterion, the jet is a region where $P_{dx} > 0.25 \cdot P_{dsw}$ with a maximum value higher than $0.5 \cdot P_{dsw}$. Furthermore, this criterion would only be applicable in the subsolar region of the magnetosheath since the magnetosheath velocity in the flanks increases with respect to the solar wind velocity, and this inequality would be satisfied almost all the time. A summary of these criteria can be viewed in Table 1.

In this work, a jet event is a time interval where P_{dx} is greater than $0.4 \cdot P_{dsw}$ for all measurement points and the maximum P_{dx} in this interval is greater than P_{dsw}. As a result, 1400 jets are selected based on these criteria. According to *Archer and Horbury* (2013), jets are only considered when the maximum dynamic pressure (P_d) of the jet is greater than twice the 20 min temporal average of the surrounding magnetosheath dynamic pressure. Our selected events show excellent agreement with this criterion.

Localized structures with an electron density of at least 50% higher than the surrounding plasma were termed as plasmoids by *Karlsson et al.* (2012). According to *Gunell et al.,* (2012, 2014), plasmoids are associated with an increase in flow velocity. Plasmoids with velocity changes of more than 10% were termed fast plasmoids by *Karlsson et al.,* (2012, 2015). Only half of the selected events in our study fully meet this criterion. In the present paper, we refer them as “fast plasmoids”.

The upstream solar wind parameters (i.e. magnetic field, velocity, density, temperature) were obtained from the 1 min OMNI solar wind data, propagated to the bow shock nose and consisted of measurements from different spacecraft around the L1 point. For instance, to compensate the uncertainty of the solar wind propagation from the spacecraft at the L1 point to the bow shock as well as to the jets locations, all upstream solar wind parameters were calculated by averaging the data 4 minutes before and after the observations of jets. To obtain the radial distance between the bow shock and the spacecraft as well as the local bow shock normal, the calculated solar wind parameters were compared with the *Farris and Russell,* (1994) bow shock model.

3 Observations

Early studies of jets in the magnetosheath have indicated that the jet formation is closely related to processes in the foreshock region of quasi-parallel bow shock. In contrast to what was reported by *Plaschke et al.,* (2013), our dataset shows that jet occurrence downstream of the quasi-perpendicular shock is not uncommon. However, one should note

171 that we have used a somewhat different selection criterion, and the jets in our dataset show
172 higher anti-sunward velocity enhancements. Figure 1a presents the histogram of the relative
173 probability of the jet observation with respect to the θ_{Bn} and cone angles, represented by red
174 and blue colored lines respectively. Figure 1a shows that such jets are observed in a wide
175 range of θ_{Bn} and cone angles but are primarily observed during typical Parker's spiral IMF
176 (i.e. cone angles ~ 45°).

177 On the other hand, the θ_{Bn} angle highly affects the propagation of the jets. Figure 1b
178 presents a scatter plot of the radial jet to bow shock distance as a function of the local θ_{Bn}
179 angle, represented in blue-colored dots. The red-colored dots are the median values in each
180 0.5 R_E bin. The plot indicates clear decreasing trend of the θ_{Bn} angle, with respect to the
181 distance from the bow shock. As shown in Figure 1b, jets can be observed in a wide range of
182 radial distance to the bow shock, however, it is noteworthy to mention that jets downstream
183 of the quasi-perpendicular shock were observed only up to 2.5 R_E.

184 Figure 1c presents a map of the jets location in XR_{GSE} plane, where $R_{GSE}=\sqrt{Y_{\mathrm{GSE}}^2+\mathrm{Z}_{\mathrm{GSE}}^2}$
185 in the geocentric solar ecliptic (*GSE*) coordinate system. In this figure, the locations of the
186 jets are separated based on whether they are observed in the regions of quasi-parallel or
187 quasi-perpendicular magnetosheath. Jets that are observed downstream of quasi-parallel
188 (quasi-perpendicular) shock are plotted in the positive (negative) R_{GSE} region. The colored
189 dots correspond to different ranges of the radial distance of the jets to the model bow shock
190 locations. It is clearly observable in Figures 1b-c that the jets are predominantly observed
191 closer to the bow shock (distance from the bow shock <2 R_E) than to the magnetopause.
192 Similar result is also noted in *Plaschke et al.,* (2013). *Palmroth et al.,* (2018) used a global
193 hybrid simulation and found that the dynamic pressure is greatest nearest to the shock and
194 decreases as the jets propagate towards the magnetopause. The dynamic pressure decreases
195 by 70% from the bow shock to the vicinity of the magnetopause. This effect indicates that the
196 origins of the jet may be related to the dynamic pressure upstream the bow shock.

197

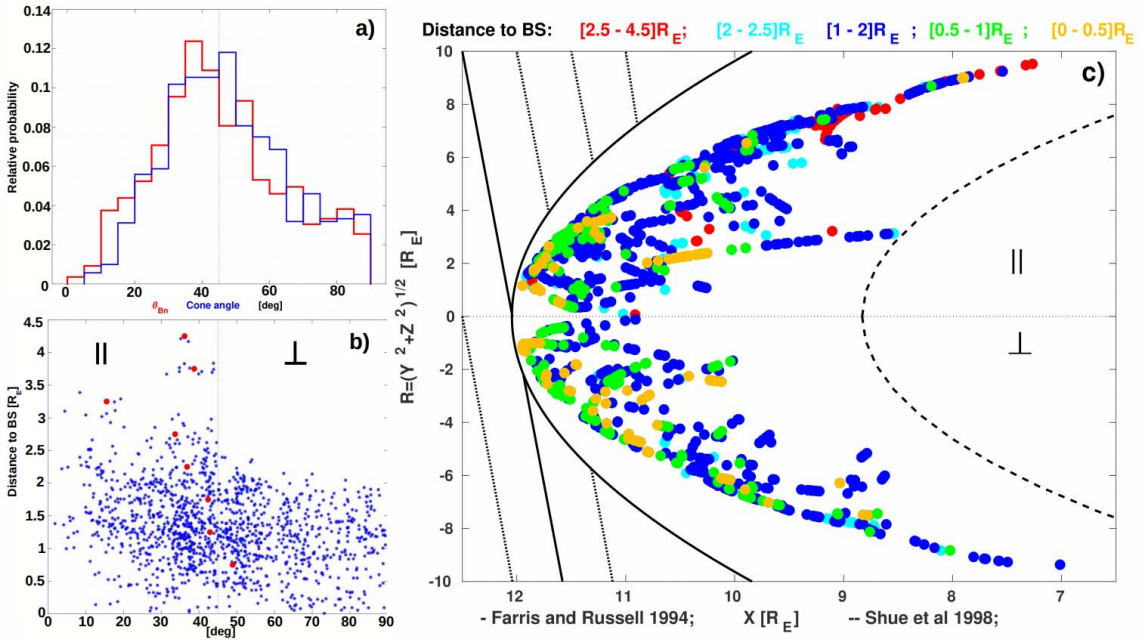

Figure 1. (a) Distributions of the local θ_{Bn} and cone angles (cos^{-1} $(B_x /|B|)$) during jet observations are represented by red and blue colored lines, respectively. (b) Distribution of the propagation depth (radial distance to the bow shock) as a function of the local θ_{Bn} angle. The red-colored dots are the median values in each 0.5 R_E bin. (c) Map of jets in the quasi-parallel (R>0) and quasi-perpendicular magnetosheath (R<0) in the XR_{GSE} plane. Parabolas indicate modeled position of bow shock (*Farris and Russell,* 1994) and magnetopause (*Shue et al.,* 1998). Color coding corresponds distance to the bow shock.

Our statistical analysis is based on MMS observations in the magnetosheath. 1400 jets were selected in this work and as shown in Figure 1b, about 35% of the events were observed downstream of the quasi-perpendicular bow shock. One example of such events is shown in Figure 2. On October 25, 2015, the MMS spacecraft were located at [10.05; 6.47; -0.67] R_E. OMNI cone angle is shown in Figure 2a and the magnetosheath parameters (i.e. plasma velocity along the Earth-Sun line, ion energy-time spectrogram of energy flux and dynamic pressure) from MMS1 spacecraft in fast mode are shown in Figures 2b-d. The cone angle of the entire interval shown in Figure 2a is always greater than 50 degrees suggesting that the spacecraft is located downstream of the quasi-perpendicular bow shock. In addition, the rather narrow ion energy range shown in Figure 2c is a typical characteristic of the quasi-perpendicular magnetosheath. Furthermore, according to the *Farris and Russell* (1994) bow shock model, the spacecraft were located approximately 0.85 R_E from the bow shock, with local bow shock normal $\boldsymbol{n}$=[0.95; 0.23; -0.16] and θ_{Bn} = 70°.

At around 10:18 UT (the red-boxed region in Figure 2a-d), three jets with rapid increases/enhancements in the X-component of plasma velocity and the total dynamic pressure were identified (i.e., Figure 2b and d). The high-time resolution plasma measurements (burst mode) of this interval are expanded and presented in Figure 2e-l. Due to the close MMS spacecraft configuration on this particular date which are in the order of a

few tens of kilometers (i.e., much smaller than the typical scale sizes of jets), measurements of all spacecraft are almost the same (see Figure 2h and k). Hence, only data from MMS1 are shown here.

The number of jets identified is highly sensitive to the selection criteria. The application of a different selection criterion over the same time interval as shown in Figure 2e-l could result in a different number of jets. For instance, the criterion used by *Archer and Horbury* (2013), if applied here, would have identified the five jets which are marked by the blue and yellow dashed lines in Figure 2e-l. On the other hand, the initial criterion of *Plaschke et al.,* (2013) would have identified four of these jets, and three of them (marked by blue dashed lines) matched the identified jets in this work. On the contrary, only two (marked by yellow dashed lines) of these five jets would have been identified if the plasmoid selection criterion by *Karlsson et al.,* (2015) had been applied instead. The different discussed criteria are reflected in Figure 2k and l.

In a case study, *Eriksson et al.,* (2016) observed a high current density inside a jet and concluded that a current sheet had formed at the boundary between colder, more solar wind-like plasma and warmer, magnetosheath-like plasma. The current sheet, as well as the jet, propagated from the bow shock toward the magnetopause. Similar to previously reported jets which predominantly have been observed in the quasi-parallel magnetosheath (e.g. *Plaschke et al.*, 2013; *Eriksson et al.,* 2016), the jets we identify in this work, downstream of quasi-perpendicular shock, are also associated with current density enhancements (Figure 2g). In Figure 2j, it is seen that the ion energy flux is high inside the jets, peaking at an energy of ~0.8 keV which is not far below the typical solar wind proton energy of ~1keV. However, these signatures can also be observed for "small jets" that do not match any of the criteria discussed in this work, for example in the approximate period from 10:17:36 to 10:17:46 UT as shown in Figure 2j. Hence, jets should not be identified based solely on one single parameter. A comparison of the energy flux with signatures in other measured quantities is more likely to provide a good identification criterion.

Based on the magnetic field strength compared to the surrounding background field, *Karlsson et al.,* (2015) divided the plasmoids they observed into two distinct groups. Plasmoids that were associated with clear magnetic field increases were called "paramagnetic" and plasmoids with clear decreases were called "diamagnetic". The majority of the jets and fast plasmoids identified in our dataset have paramagnetic signatures. However, it is of interest to note that the magnetic field signatures within the jets and fast plasmoids themselves are not always same. For instance, it is shown in Figure 2e that the magnetic field of the jets (boxes with blue dashed lines) are accompanied with larger fluctuations and more rapid rotations compared to the fast plasmoids (boxes with yellow dashed lines).

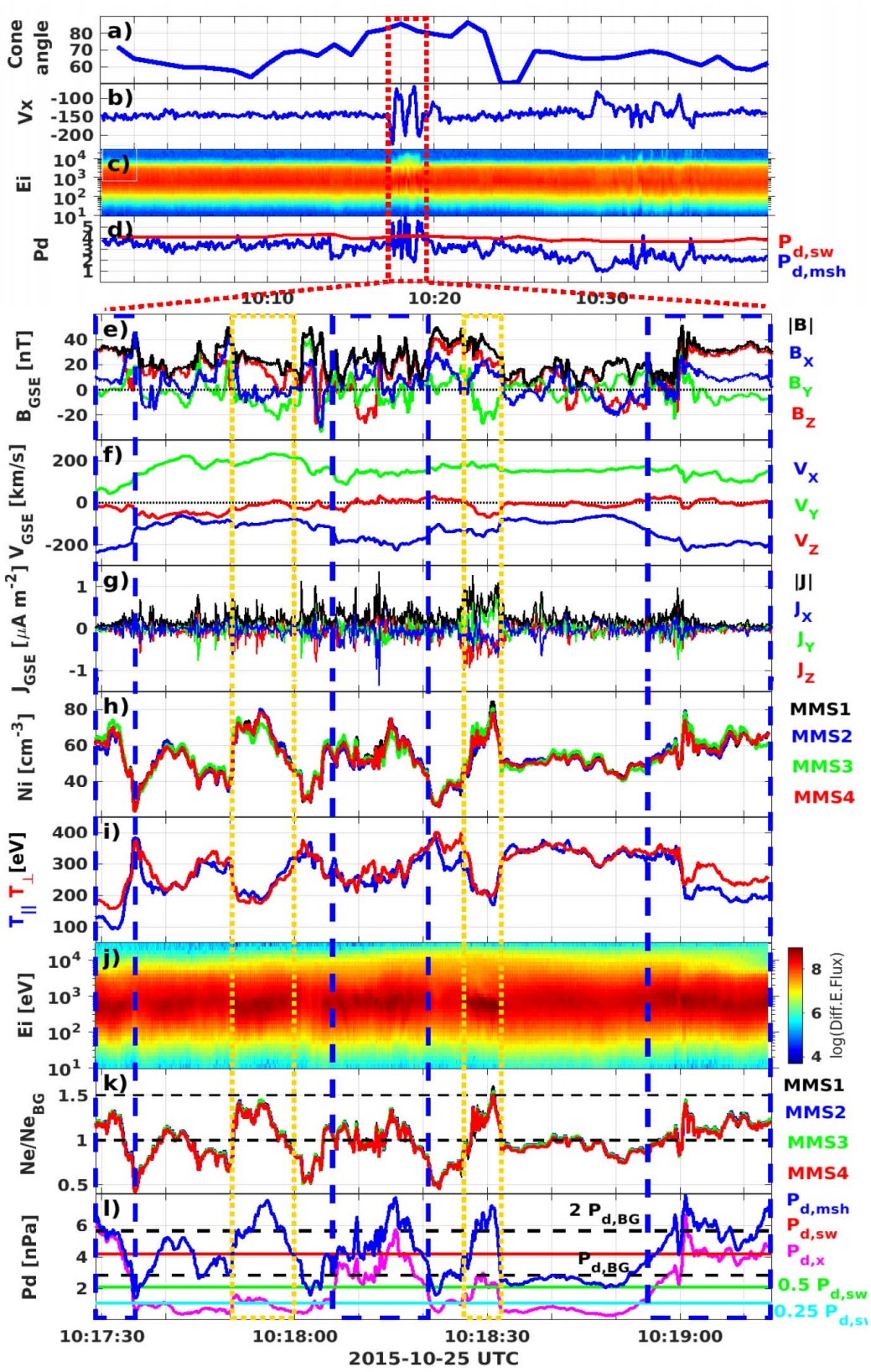
a)
Cone angle
b)
Vx
c)
Ei
d)
Pd
P d,sw
P d,msh
10:10
10:20
10:30
e)
B GSE [nT]
|B|
B X
B Y
B Z
f)
V GSE [km/s]
V X
V Y
V Z
g)
J GSE [μA m-2]
|J|
J X
J Y
J Z
h)
Ni [cm-3]
MMS1
MMS2
MMS3
MMS4
i)
T|| T⊥ [eV]
j)
Ei [eV]
log(Diff.E.Flux)
k)
Ne/Ne BG
l)
Pd [nPa]
2 P d,BG
P d,BG
P d,msh
P d,sw
P d,x
0.5 P d,sw
0.25 P d,sw
10:17:30
10:18:00
10:18:30
10:19:00
2015-10-25 UTC

Figure 2. The orientation of the IMF with respect to the Earth-Sun line propagated to the nose of bow shock (a) and (b-d) MMS1 observations in the magnetosheath on October 25, 2015. (e-l) Enlarged intervals of the box with red dash lines showing a series of the jets in the x-component of velocity. The ion density (h) and electron density ratio (k) are shown from all four spacecraft. The last two panels indicated the identification criteria of (k) *Karlsson et al.,* (2015) (yellow boxes), (l) *Archer and Horbury* (2013) (both yellow and blue boxes) and (l) *Plaschke et al.,* (2013) (blue boxes). See the main text for descriptions of each method.

On the other hand, the changes in the ion and electron densities of the jets and plasmoids show excellent anti-correlation with the changes in ion temperature (comparing Figures 2h and k to Figure 2i). Such a signature is observed in all 1400 cases (results not shown) and is consistent with the study by *Gutynska et al.*, (2015), who analyzed jets based on density enhancements using a criterion similar to that of *Karlsson et al.,* (2012). An anti-correlation between density and temperature is a typical signature of magnetosonic waves. In other words, these results suggest that jets and fast plasmoids are magnetosonic in nature.

4 Upstream and downstream conditions

Apart from the clear dependence on cone angles, *Plaschke et al.,* (2013) pointed out that jets in the quasi-parallel magnetosheath have rather weak to insignificant dependence on solar wind velocities and magnetic field strengths. Figures 3 shows histograms of the upstream solar wind parameters: (a-d) magnetic field components and magnitude, (e) plasma velocity magnitude, (f) dynamic pressure, (g) Alfvén mach number ($M_A=|V|/V_a$, where $V_a=|B|/\sqrt{\mu_0\rho}$ is the Alfvén speed and μ_0 the vacuum permittivity) and (h) plasma beta ($\beta=2\mu_0 k_B NT/|B|^2$, where k_B is Boltzmann's constant, N the solar wind density, and T is the solar wind temperature), at the time when the jets were observed in quasi-parallel (green lines) and quasi-perpendicular (red lines) magnetosheath. In all panels, the blue lines show the respective parameters in the entire time periods regardless of whether jets were identified**.** Figures 3a-c show that there is no (clear) dependence between the jet occurrence and the IMF orientations. In Figure 3d and e, the difference between the blue and green distributions shows that the occurrence of jets in the quasi-parallel magnetosheath have clearer dependence on the magnitude of both the magnetic field and plasma velocity. In addition, our results show that the occurrence of jets in the quasi-perpendicular magnetosheath is linked to higher (about 20%) solar wind magnetic field and plasma velocity magnitudes than jets in the parallel magnetosheath. Similar dependence can also be observed in the dynamic pressure and Alfvén mach number shown in Figure 3f and g. Furthermore, in contrast to *Plaschke et al.,* (2013), the occurrence of jets in our work shows strong dependence on the solar wind plasma beta. In particular, higher plasma beta is observed when jets are present in the magnetosheath. The plasma beta is 30% higher when the jets are observed in the quasi-perpendicular magnetosheath compared to quasi-parallel magnetosheath (red and green lines in Figure 3h).

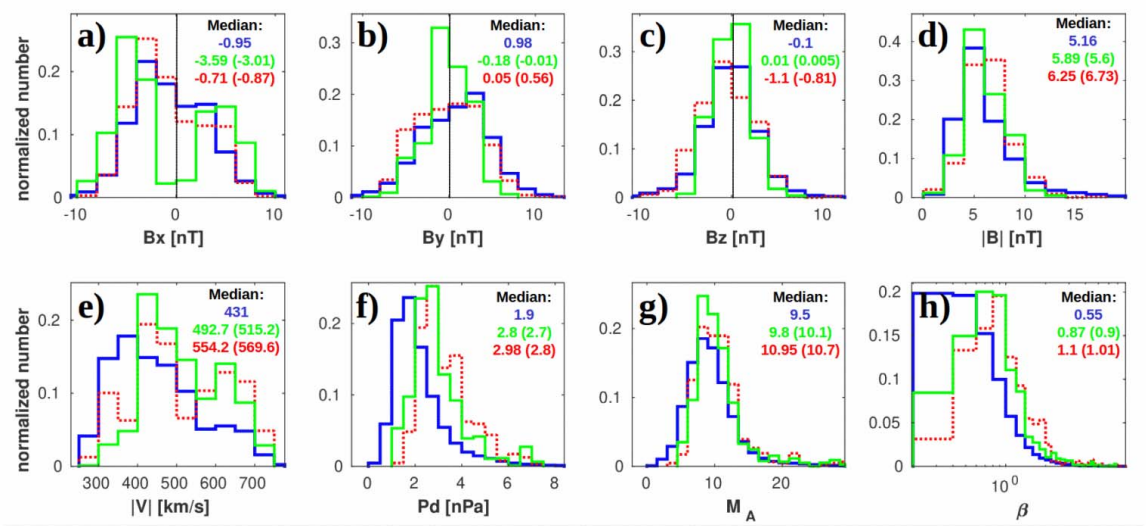

Figure 3. Distributions of the upstream solar wind parameters during October 2015 - January 2016, and October 2016 – February 2017. (a)-(c) *XYZ* components of the IMF; (d) total solar wind magnetic field; (e) total velocity of the solar wind; (f) total solar wind dynamic pressure; (g) Alfvén Mach number ; (h) plasma beta. The values in brackets correspond to fast plasmoids, and colors represent jets in the quasi-parallel (green) and quasi-perpendicular (red) magnetosheath. The blue lines show the distribution for the whole observational interval, that is to say, both inside and outside the jets.

Figure 4 shows the change in direction of the magnetic field and the plasma bulk velocity between the solar wind, the magnetosheath, and the jets. Figure 4a shows a histogram of the angle between the magnetic field in the solar wind and in the magnetosheath, and in Figure 4b a histogram of the angle between the velocity vector in the solar wind and in the magnetosheath is shown. Figure 4c shows how the median of these angles varies with the distance to the bow shock. In all panels the quasi-parallel magnetosheath is shown in green and the quasi-perpendicular in red. Changes of the IMF orientation in the quasi-perpendicular magnetosheath are smaller (red line in Figure 4a) than in the quasi-parallel magnetosheath. *Dimmock and Nykyri* (2013) showed that the quasi-perpendicular magnetosheath is a region favorable to magnetic field and velocity asymmetry (i.e., velocity and magnetic field strength are larger on the dusk flank), during typical Parker's spiral IMF. However, deflections of the plasma flow in the quasi-parallel and quasi-perpendicular magnetosheath are almost the same (Figure 4b). The triangles and circles in Figure 4c show that the deflection of the IMF and plasma flow from the solar wind orientation increases with the propagation depth in the sheath. Due to higher fluctuations in the quasi-parallel magnetosheath, calculation errors of the magnetic field rotation are rather large (green triangles).

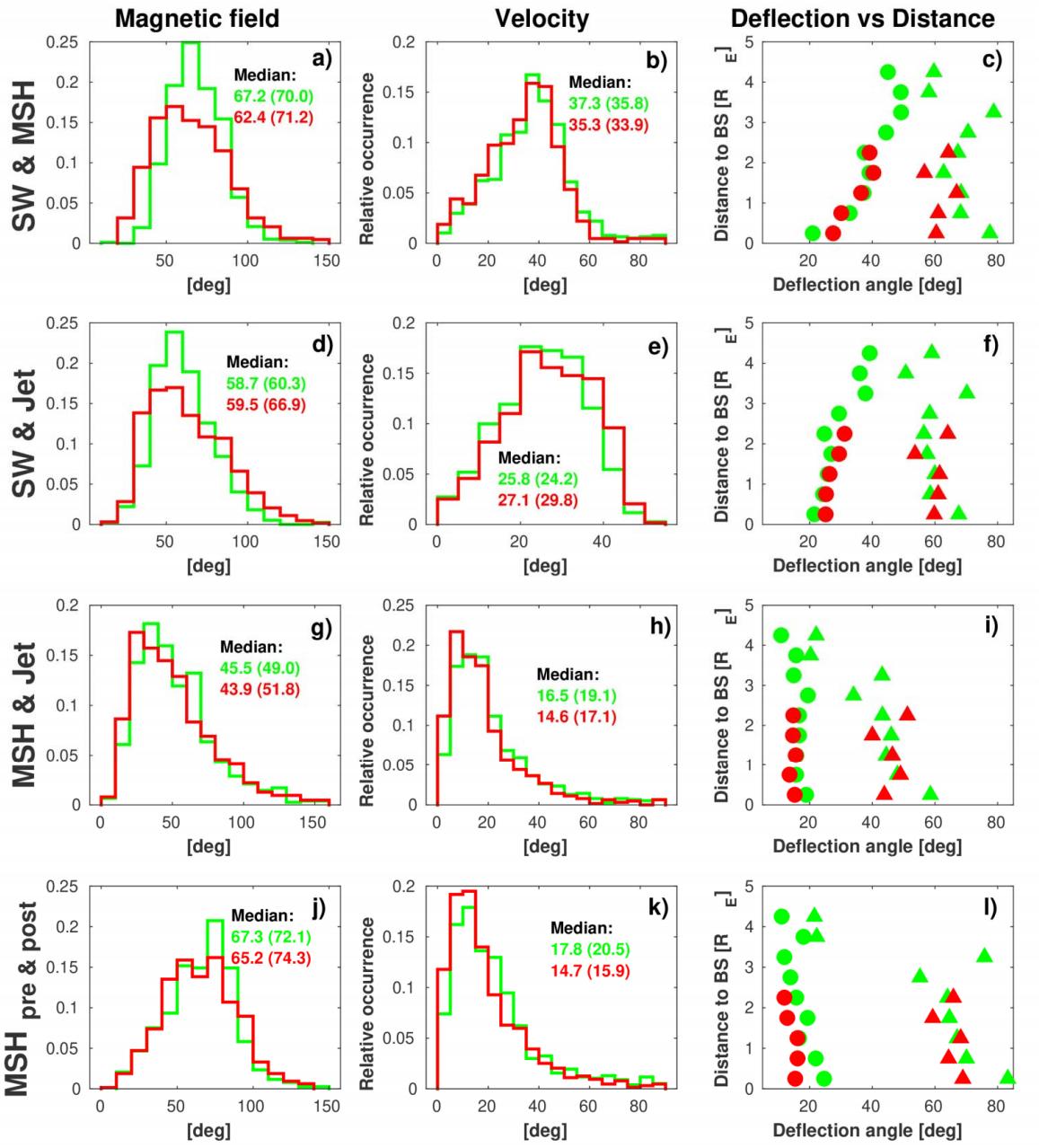

Figure 4. Histograms of the magnetic field (left column) and plasma flow (middle column) deflections in different regions of the magnetosheath. Changes of the deflection angles with the distances to bow shock are shown in the right column. The panels a-c and d-f presents changes of the solar wind parameters in the magnetosheath (SW&MSH), and inside jet (SW&Jet). Differences of the magnetosheath parameters inside (MSH&Jet) and around ($MSH_{pre\&post}$) jets are presented in panels g-i and j-l, respectively. In all panels, the green and red colors represent the quasi-parallel and the quasi-perpendicular magnetosheath, respectively. Filled circles correspond to velocity deflections and filled triangles to magnetic field deflections.

We find that the median deflection of the solar wind flow from the Sun-Earth line is 2.68 degrees (not shown). Previous studies concluded that the velocity of magnetosheath jets is generally oriented more along the Sun-Earth line i.e similar with the solar wind flow (*Gunell et al.,* 2012; *Hietala et al.*, 2012; *Hietala and Plaschke* 2013; *Archer and Horbury* 2013; *Plaschke et al.,* 2013). Figures 4d-f show the changes of the jet plasma flows, as well as the magnetic fields, from the solar wind orientation. That the deflection angle increases with bow shock distance, as shown by the colored circles in Figure 4f, leads to the conclusion by *Gunell et al.,* (2012), that the plasmoids move predominantly in a tangential direction.

On the other hand, *Hietala and Plaschke* (2013) reported that the jets have a tendency to continue 'straight' along the Sun–Earth line as compared to the background magnetosheath flow. The deflection from the background magnetosheath flow is in the range of 20° to 45°. *Plaschke et al.,* (2013) reported a number of 28.6° for the median deflection. In our statistics, the median deflection for both types of jets are quite similar and in a good agreement with early reported range (Figures 4g-h). However, according to *Archer and Horbury* (2013), the deflections from the magnetosheath flow are typically only a few degrees. Study of the overlap between *Plaschke et al.,* (2013) and *Archer and Horbury* (2013) definitions showed agreement only in 17 % of the events (*Vuorinen et al.*, 2019). Probably, this means that the *Archer and Horbury* (2013) criterion include not only jets but the numbers of the other structures, close to the magnetopause. Figure 4i shows that differences of the magnetic field (triangles) and flow (circles) orientations inside and outside of the jet decreases with propagation depth.

Propagating through the magnetosheath, jets do not only affect the magnetopause and magnetosphere. Simulation results by *Karimabadi et al.,* (2014) showed that jets pushed slower ambient magnetosheath plasma out of their way. As a result, plasma moves around the jets, and it is slowed down or could even be pushed in the sunward direction. Consequently, jets may create anomalous flows and be a source of additional turbulence. Figure 4k shows a histogram of the angle between the magnetosheath flow direction ahead and behind the jets. In this work, the majority of the jets are associated with small changes in the magnetosheath flow. However, from Figure 4j it can be seen that jets are accompanied by strong changes in the magnetosheath magnetic field orientation. On the other hand, the influence of the jets on the surrounded magnetosheath decreases with the propagation distances (Figure 4l).

The magnetosheath jet velocity is considerably greater than the local Alfvén velocity. Some jets are also supermagnetosonic and may even be associated with a local shock at the front of the jet (*Plaschke et al.,* 2017; *Plaschke and Hietala,* 2018; *Hietala et al*., 2009, 2012). In our analysis, about 95% of jets are superalfvénic (not shown) with median Alfvénic Mach number of 1.8 in the quasi-parallel and 1.6 in the quasi-perpendicular magnetosheath. Nevertheless, only 12% of them are supermagnetosonic (i.e. jet speed is higher then magnetosonic speed, $V_{ms}=\sqrt{V_A^2+C_s^2}$, where $C_s = \sqrt{\gamma k_B (T_e+T_i)/(m_i+m_e)}$is the sound speed, γ is the adiabatic index). *Plaschke et al.,* (2013) noted that in the subsolar region, only about 14% of jets are supermagnetosonic. *Archer and Horbury* (2013) suggested that the majority of the supermagnetosonic jets must be observed in the flanks of the magnetosheath. On the other hand, they pointed out that density driven jets are more likely to occur at the flanks. The global electromagnetic hybrid simulations of the structures with density enhancements by *Omidi et al.,* (2014) predicted their propagation into the magnetosheath at the flanks. The small apogee of the MMS orbit during the entire period do not allow a clear conclusion about

jets at the flanks. Further analysis of the MMS measurements at the magnetosheath flanks on 2017-2018 is necessary and should be done in the near future.

Covering the whole day side region, *Archer and Horbury* (2013) reported that there is no clear change in observation probability with distance from the bow shock. The analysis of plasmoids in the magnetosheath by *Karlsson et al.,* (2015) showed that plasmoids with changes in velocity are found for X_{GSE}>2 R_E, while plasmoids without velocity changes (labeled embedded plasmoids by *Karlsson et al.,* (2015)) are found further downstream for X_{GSE}>-5 R_E. Figures 1b-c and 4f,i show that velocity driven jets are more common close to the bow shock and deflections from the magnetosheath flow decrease with increasing propagation distances. Such an effect can be the result of jets slowing down, while propagating through the magnetosheath. Figure 5 shows the ratio of jet speed to magnetosheath flow speed as a function of bow shock distances for jets and fast plasmoids in the quasi-parallel and quasi-perpendicular magnetosheaths. In the quasi-parallel magnetosheath as well as in the quasi-perpendicular, the median values in each 0.5 R_E distance bins show a signature of the jets and fast plasmoids slowing down. Similar signatures were observed by *Dmitriev and Suvorova* (2015), who followed jets with the five THEMIS spacecraft and reported a decrease of the jet velocity as it moved towards the magnetopause. Differences of the deceleration trend in the quasi-perpendicular and quasi-parallel magnetosheath can be connected with the formation mechanisms and the asymmetry of the magnetosheath magnetic field and velocity, associated with a quasi-perpendicular bow shock (*Dimmock and Nykyri*, 2013).

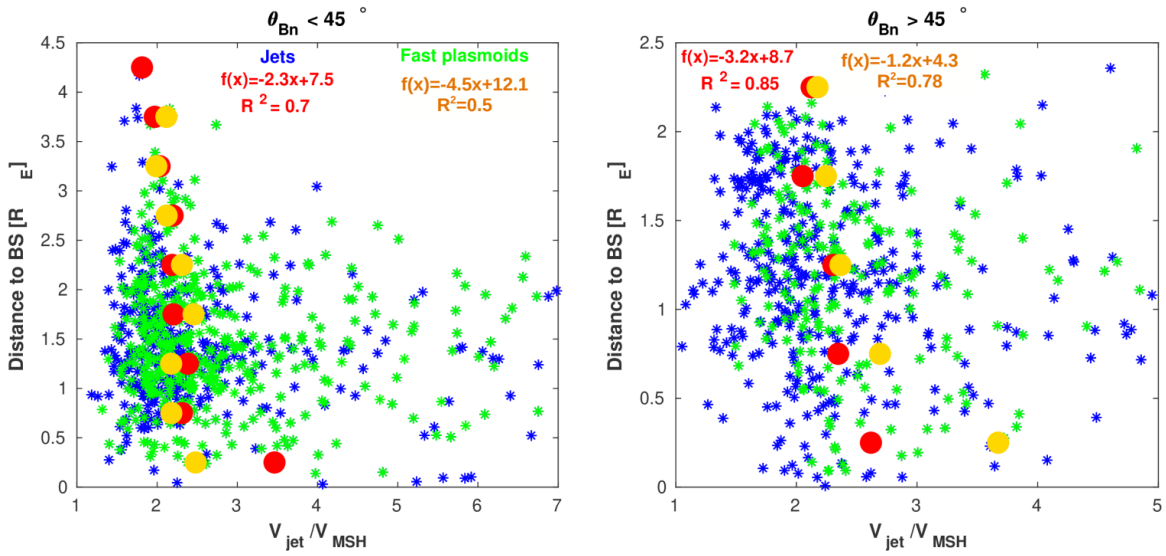

Figure 5. Changes of the flow velocities inside jets (blue) and fast plasmoids (green) regarding to the local speed with bow shock distances in the quasi-parallel (left) and quasi-perpendicular (right) magnetosheath. The median values of jets and fast plasmoids in each 0.5 R_E bin are marked by red and yellow dots, respectively.

5 Discussion

We have presented a statistical study of magnetosheath jets and fast plasmoids in the quasi-parallel and quasi-perpendicular magnetosheath. We compared the main observational

411 criteria used in the past (*Plaschke et al.,* 2013; *Archer and Horbury*, 2013; *Karlsson et al.,*
412 2012, 2015) and we could verify the properties of jets and fast plasmoids. Our results mainly
413 confirmed previous statistical studies and shows good agreement between jets and fast
414 plasmoids. However, we showed that jets occur not only downstream of the quasi-parallel
415 shock and that jets in the quasi-perpendicular magnetosheath are not rare. In contrast to
416 *Plaschke et al.,* (2013), we found that the occurrence of jets is not exclusive to low IMF cone
417 angles and they can be detected even during a perpendicular IMF orientation. The existence
418 of jets in the quasi-perpendicular magnetosheath is mainly connected with oblique IMF
419 orientations. A strong solar wind with higher than average velocity and magnetic field (i.e.,
420 higher Alfvén Mach number and plasma beta) creates conditions favorable for the generation
421 of jets.

422 As they propagate through the magnetosheath, the jets push the ambient
423 magnetosheath plasma out of their way and are slowed down in the process. *Dmitriev and*
424 *Suvorova* (2015) discussed a large-scale jet whose velocity decreased about 20% over a 1.4
425 R_E propagation distance in the magnetosheath. The trends in Figure 5 show a quite fast
426 deceleration rate in both the perpendicular and parallel magnetosheath. According to the best
427 fit equation in our results, at distances of about 5-7 R_E from the bow shock, both jets and fast
428 plasmoids have acquired the same velocity as the surrounding magnetosheath. Such fast
429 deceleration of jets and plasmoids in the magnetosheath can explain the results of *Karlsson et*
430 *al.* (2015), who pointed out that plasmoids were observed up to X_{GSE} = -5 R_E, but fast
431 plasmoids only until X_{GSE} = 2 R_E.

432 What mechanism leads to the formation of jets is still under debate. Many different
433 models have been suggested. The majority of these conclude that foreshock processes are
434 responsible for generating most of the jets (*Plaschke et al.,* 2013; *Hietala et al.*, 2012;
435 *Hietala and Plaschke* 2013). Among the more notable of the suggested mechanisms we find
436 *bow shock ripples* and *SLAMS* which are both inherent to the quasi-parallel shock, although
437 ripples have also bee observed on the quasi-perpendicular shock (*Johlander et al.* 2018). On
438 the other hand, *Archer et al.* (2012) suggested that jets could form when the shock locally
439 changes from quasi-parallel to quasi-perpendicular or vice versa due to IMF discontinuities
440 passing the bow shock. However, jets are mostly observed during steady IMF and only 15%
441 of the jets in this study were connected with a clear signature of a solar wind discontinuity.
442 For this reason, alternative formation mechanisms are also needed to explain the
443 observations.

444 Early estimates of the size of the magnetosheath jets gave values in the order of 1 R_E
445 (*Archer et al.,* 2012; *Karlsson et al.,* 2012, 2015; *Hietala et al*., 2009, 2012; *Gutynska et al.*,
446 2015). However, reports of the detailed morphology of the jets have been somewhat
447 inconsistent. *Archer et al.,* (2012) report a longer scale size parallel to the jet flow than
448 perpendicular to it. *Plaschke et al.,* (2016) interpreted his results as the jets having a pancake-

like geometry. Similar to previous studies, we assumed a cylindrical jet geometry. The dimension along the flow direction ($D||$) was estimated for every jet and fast plasmoid observation by integrating the ion velocity over the jet duration (Δt). The duration times were determined as the time of jet observation, where the P_{dx} is greater than $0.4 \cdot P_{dsw}$. An upper limit of the flow parallel size was proposed by *Gunell et al.,* (2014) as the product of the duration and maximum speed, and this provide excellent agreement with $D||$ in the all distance ranges (not shown).

To determine thickness (Dp) of jets, we use the Rankine-Hugoniot relations (*Koval and Szabo,* 2008) to obtain the local normal and speed along this estimated normal. In particular, we require the angle between the obtained normal and the jet flow direction to be in the 80° to 100° range. Applying these criteria, we obtain a set of 980 cases of jet and fast plasmoid observations in the quasi-parallel and quasi-perpendicular magnetosheath. Assuming that the jet propagated along the normal with the estimated speed, the jet thickness was calculated. The thickness is an over-estimate as we have not take into account propagation parallel to the flow (V_{jet}). Figure 6 shows a sketch of our assumption. The spacecraft is located on top, and the estimated trajectory of its motion is shown by dashed colored lines.

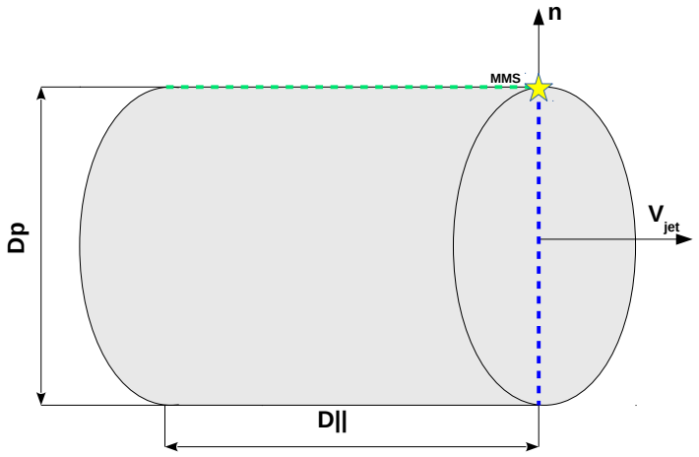

Figure 6. Conceptual figures of the jet morphology. The assumed position of the spacecraft is shown by a yellow five-pointed star. The green dashed line shows the trajectory of the jet crossing when it moves parallel to the plasma flow. The trajectory of the cross scale size estimation is represented by a blue dashed line.

Table 2 shows the median values of the jet and fast plasmoid sizes in the quasi-parallel and quasi-perpendicular magnetosheath, at different distances from the bow shock. The last row in Table 2 represent the median values over all 980 events, regardless their location in the magnetosheath.

475 **Table 2.** Perpendicular (*Dp*) and parallel (*D*||) scale sizes of the jets (HSJ) and fast plasmoids
476 (FP) at different distance ranges. The median sizes, regardless distance from the bow shock
477 are shown in the last row.

Distance to BS, R_E	Quasi-parallel MSH				Quasi-perpendicular MSH			
	HSJ		FP		HSJ		FP	
	Dp	D||	Dp	D||	Dp	D||	Dp	D||
0-0.5	0.43	1.24	0.43	1.11	0.39	1.05	0.34	0.99
0.5-1	0.45	1.19	0.43	1.18	0.43	1.11	0.56	1.35
1-1.5	0.62	1.36	0.73	1.53	0.60	1.48	0.76	1.75
1.5-2	0.67	1.38	0.78	1.68	0.74	1.64	0.85	2.45
2-2.5	0.66	1.47	1.03	1.88	0.72	2.45	0.72	3.23
2.5-3	0.95	1.56	1.01	2.05	-	-	-	-
3-3.5	1.88	6.19	1.35	6.72	-	-	-	-
3.5-4	2.74	4.42	1.92	4.05	-	-	-	-
4-4.5	3.04	4.50	-	-	-	-	-	-
Median	0.63	1.07	0.72	1.22	0.56	1.09	0.69	1.24

478 Figure 7 shows how the parallel and perpendicular scale sizes change with the
479 distance from bow shock. The colors of the small stars represent type of the magnetosheath,
480 and the median values in each 0.5 R_E bin are shown by filled red and yellow circles. Both
481 plots indicate continuous increasing trends of the parallel, *D*|| (left), and perpendicular, *D*p
482 (right), dimensions of jets in the quasi-parallel (blue) and quasi-perpendicular (green)
483 magnetosheath. The values in Table 2 show that the extent of both jets and fast plasmoids
484 parallel to the direction of propagation is almost twice as high as the perpendicular extent
485 irrespective of magnetosheath type. A similar conclusion was reported by *Archer et al.,*
486 (2012). However, the slopes of the curves described by the red and yellow circles,
487 respectively, indicate that the jets expand faster in the perpendicular than the parallel
488 direction as they travel through the magnetosheath. Similar results were observed for fast
489 plasmoids (not shown) and confirmed the conclusion by *Karlsson et al.* (2015) that the
490 plasmoids are a subset of magnetosheath jets.

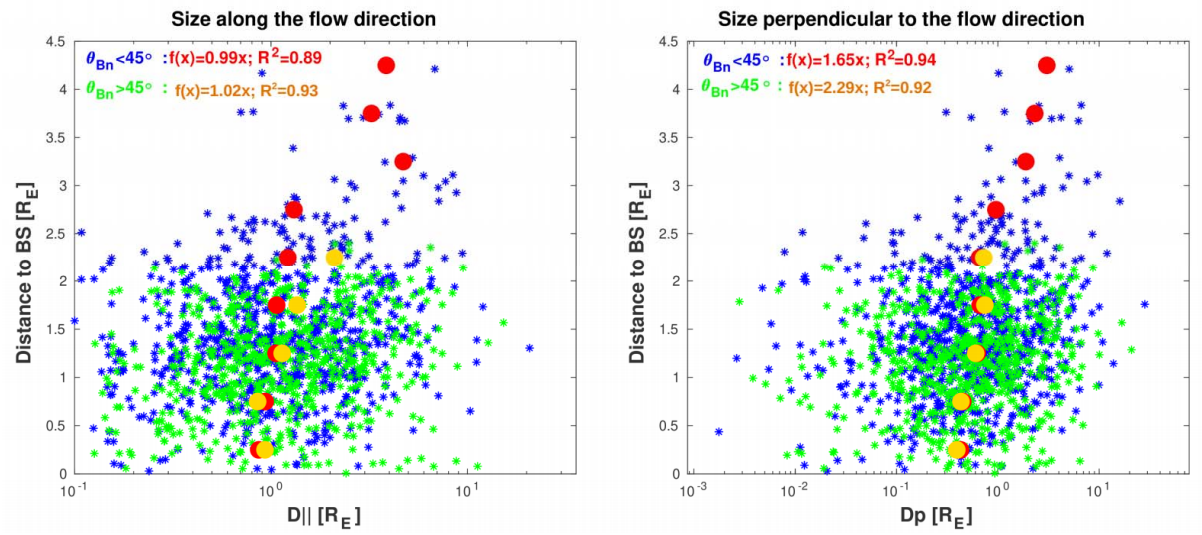

Figure 7. Scatter diagrams of jet observations in a size-distance plane. The left panel shows the length parallel to the direction of propagation and the right panel shows the jet extent in the dimension perpendicular to the direction of propagation. The small blue and green stars represent observations in the quasi-parallel and quasi-perpendicular magnetosheath, respectively. The large filled red and yellow circles show median values in each 0.5 R_E bin.

6 Summary and Conclusion

Based on our analysis of 1400 events, with higher enhancements in the x-component of the velocity, in a broad range of the magnetosheath and upstream parameters, we can summarize our conclusions in the following list.

- The basic properties of jets and fast plasmoids are very similar.
- The probability of jet generation increases when the solar wind is stronger, i.e. when it has a higher velocity, magnetic field, Alfvén mach number and plasma beta.
- Jet observations in the quasi-perpendicular magnetosheath are relatively common.
- Jet observations are more frequent close to the bow shock, and their direction is toward the magnetopause.
- A low θ_{Bn} angle enables propagation deeper into the magnetosheath.
- The propagation speed of a jet decreases as it moves towards the magnetopause, and during its propagation, the velocity of the jet tends toward the velocity of the surrounding magnetosheath.
- The typical size of these structures is several thousands of kilometers and it increases with the distance to bow shock.
- The parallel size of the jets and plasmoids is almost two times higher than perpendicular size, in both the parallel and perpendicular magnetosheath.

Our comparative analysis showed no significant differences between the plasma properties of the jets and fast plasmoids. However, the different magnetic fields inside the structures, suggest that the formation mechanisms are different. *Palmroth et al.,* (2018), found that the

criteria applied by *Archer and Horbury* (2013) and *Karlsson et al.* (2012) provide a better opportunity than the criterion by *Plaschke et al.* (2013) to detect jets "shaped more like blobs". Further comparative analysis of the detailed structure of these plasmoids and jets is necessary and will be conducted in the near future.

Acknowledgments

OG was supported by the Kempe foundation, HG by the Belgian Science Policy Office through the Solar Terrestrial Centre of Excellence and by the Swedish National Space Agency (SNSA) grant 108/18, and MH by SNSA. We thank the MMS Science Data Center and all the MMS teams, especially the magnetic field and the ion teams, in producing high quality data. We also acknowledge NASA's National Space Science Data Center and Space Physics Data Facility. All data are available through https://omniweb.gsfc.nasa.gov/ and https://lasp.colorado.edu/mms/sdc/public/.

References

Archer, M.O., Horbury,T.S., Eastwood, J.P., Magnetosheath pressure pulses: generation downstream of the bow shock from solar wind discontinuities. J. Geophys. Res. 117, 05228 (2012). https://doi.org/10.1029/2011JA017468

Archer, M. O. and Horbury, T. S.: Magnetosheath dynamic pressure enhancements: occurrence and typical properties, Ann. Geophys.31, 319–331, https://doi.org/10.5194/angeo-31-319-2013, 2013.

Blanco-Cano, X., Omidi, N., Russell, C.T., Macrostructure of collisionless bow shocks: 2. ULF waves in the foreshock and magnetosheath. J. Geophys. Res. 111(A10), 10205 (2006a). https://doi.org/10.1029/2005JA011421

Blanco-Cano, X., Omidi, N., Russell, C.T., ULF waves and their influence on bow shock and magnetosheath structures. Adv. Space Res. 37, 1522–1531 (2006b). https://doi.org/10.1016/j.asr.2005.10.043

Burch, J. L., Moore, T. E., Torbert, R. B., and Giles, B. L.: Magnetospheric Multiscale Overview and Science Objectives, Space Sci. Rev., 199, 5–21, https://doi.org/10.1007/s11214-015-0164-9, 2016.

Burgess, D., On the effect of a tangential discontinuity on ions specularly reflected at an oblique shock. J. Geophys. Res. 94, 472–478 (1989). https://doi.org/10.1029/JA094iA01p00472

Dimmock, A. P. and Nykyri, K.: The statistical mapping of magnetosheath plasma properties based on THEMIS measurementsin the magnetosheath interplanetary medium reference frame, Journal of Geophysical Research: Space Physics, 118, 4963–4976,15 (2013). https://doi.org/10.1002/jgra.

Dmitriev, A.V., Suvorova, A.V., Large-scale jets in the magnetosheath and plasma penetration across the magnetopause: THEMIS observations. J. Geophys. Res. 120, 4423–4437 (2015). https://doi.org/10.1002/2014JA020953

Dunlop, M. W., A. Balogh, K.-H. Glassmeier, and P. Robert (2002), Four-point Cluster application of magnetic field analysis tools: The Curlometer, J. Geophys. Res., 107, 1384, doi:10.1029/2001JA005088.

562 Eriksson, E., Vaivads, A., Graham, D.B., Khotyaintsev, Y.V., Yordanova, E., Hietala, H.,
563 André, M., Avanov, L.A., Dorelli, J.C., Gershman, D.J., B.L. Giles, B. Lavraud, W.R.
564 Paterson, C.J. Pollock, Y. Saito, W. Magnes, C. Russell, R. Torbert, R. Ergun, P.-A.
565 Lindqvist, J. Burch, Strong current sheet at a magnetosheath jet: kinetic structure and
566 electron acceleration. J. Geophys. Res. Space Phys. 121(10), 9608–9618 (2016).
567 https://doi.org/10.1002/2016JA023146

568 Farris, M. H., & Russell, C. T. (1994). Determining the standoff distance of the bow shock:
569 Mach number dependence and use of models. Journal of Geophysical Research, 99,
570 17681. https://doi.org/10.1029/94JA01020

571 Goncharov, O., Safrankova, J., Nemecek, Z., Prech, L., Pitna, A., Zastenker, G.N., Upstream
572 and downstream wave packets associated with low-Mach number interplanetary shocks
573 Geophys. Res. Lett., 41 (22): 8100–8106, 2014.

574 Gunell, H., H. Nilsson, G. Stenberg, M. Hamrin, T. Karlsson, R. Maggiolo, M. André, R.
575 Lundin, I. Dandouras, Plasma penetration of the dayside magnetopause. Phys. Plasmas
576 19(7), 072906 (2012). https://doi.org/10.1063/1.4739446

577 Gunell, H., Stenberg Wieser, G., Mella, M., Maggiolo, R., Nilsson, H., Darrouzet, F.,
578 Hamrin, M., Karlsson, T., Brenning, N., De Keyser, J., André, M., and Dandouras, I.:
579 Waves in high-speed plasmoids in the magnetosheath and at the magnetopause, Ann.
580 Geophys., 32, 991–1009, https://doi.org/10.5194/angeo-32-991-2014, 2014.

581 Gutynska, O., D.G. Sibeck, N. Omidi, Magnetosheath plasma structures and their relation to
582 foreshock processes. J. Geophys. Res. Space Phys. 120, 7687–7697 (2015).
583 https://doi.org/10.1002/2014JA020880

584 Hietala, H., T.V. Laitinen, K. Andréeová, R. Vainio, A. Vaivads, M. Palmroth, T.I.
585 Pulkkinen, H.E.J. Koskinen, E.A. Lucek, H. Rème, Supermagnetosonic jets behind a
586 collisionless quasiparallel shock. Phys. Rev. Lett. 103(24), 245001 (2009).
587 https://doi.org/10.1103/PhysRevLett.103.245001

588 Hietala, H., N. Partamies, T.V. Laitinen, L.B.N. Clausen, G. Facskó, A. Vaivads, H.E.J.
589 Koskinen, I. Dandouras, H. Rème, E.A. Lucek, Supermagnetosonic subsolar
590 magnetosheath jets and their effects: from the solar wind to the ionospheric convection.
591 Ann. Geophys. 30, 33–48 (2012). https://doi.org/10.5194/angeo-30-33-2012

592 Hietala, H. and Plaschke, F.: On the generation of magnetosheath high-speed jets by bow
593 shock ripples, J. Geophys. Res., 118, 7237–7245, https://doi.org/10.1002/2013JA019172,
594 2013.

595 Hoilijoki, S., Palmroth, M., Walsh, B. M., Pfau-Kempf, Y., von Alfthan, S., Ganse, U.,
596 Hannuksela, O., and Vainio, R.: Mirror modes in the Earth's magnetosheath: Results
597 from a global hybrid-Vlasov simulation, J. Geophys. Res.-Space, 121, 4191–4204,
598 https://doi.org/10.1002/2015JA022026, 2016.

599 Johlander, A., Vaivads, A., Khotyaintsev, Y. V., Gingell, I., Schwartz, S. J., Giles, B. L.,
600 Torbert, R. B. and Russell, C. T.: Shock ripples observed by the MMS spacecraft: ion
601 reflection and dispersive properties, Plasma Phys. Control. Fusion, 60, 125006,
602 https://doi.org/10.1088/1361-6587/aae920, 2018.

Karimabadi, H., Roytershteyn, V., Vu, H. X., Omelchenko, Y. A., Scudder, J., Daughton, W., Dimmock, A., Nykyri, K., Wan, M., Sibeck, D. G., Tatineni, M., Majumdar, A., Loring, B., and Geveci, B.: The link between shocks, turbulence, and magnetic reconnection in collisionless plasmas, Phys. Plasmas, 21, 062308, https://doi.org/10.1063/1.4882875, 2014.

Karlsson, T., Brenning, N., Nilsson, H., Trotignon, J.-G., Vallières, X., and Facsko, G.: Localized density enhancements in the magnetosheath: Three-dimensional morphology and possible importance for impulsive penetration, J. Geophys. Res., 117, 03227,https://doi.org/10.1029/2011JA017059, 2012.

Karlsson, T., Kullen, A., Liljeblad, E., Brenning, N., Nilsson, H., Gunell, H., and Hamrin, M.: On the origin of magnetosheath plasmoids and their relation to magnetosheath jets, J. Geophys. Res., 120, 7390–7403, https://doi.org/10.1002/2015JA021487, 2015.

King, J.H., and N.E. Papitashvili, Solar wind spatial scales in and comparisons of hourly wind and ACE plasma and magnetic field data. J. Geophys. Res. 110, 02104 (2005).

Koval, A., & Szabo, A. (2008). Modified "Rankine-Hugoniot" shock fitting technique: Simultaneous solution for shock normal and speed. *Journal of Geophysical Research*, 113, A10110. https://doi.org/10.1029/2008JA013337

Lembège, B., Giacalone, J., Scholer, M., Hada, T., Hoshino, M., Krasnoselskikh, V., Kucharek, H., Savoini, P., and Terasawa, T. (2004), Selected problems in collisionless-shock physics, Space Sci. Rev., 110, 161.

Mazelle, C., K. Meziane, D. Le Quéau, M. Wilber, J.P. Eastwood, H. Rème, J.A. Sauvaud, J.M. Bosqued, I.Dandouras, M. McCarthy, L.M. Kistler, B. Klecker, A. Korth, M.B. Bavassano-Cattaneo, G. Pallocchia, R. Lundin, A. Balogh, Production of gyrating ions from nonlinear wave-particle interaction upstream from the Earth's bow shock: a case study from cluster-CIS. Planet. Space Sci. 51, 785–795 (2003).https://doi.org/10.1016/j.pss.2003.05.002

Němeček, Z., Šafránková, J., Přech, L., Sibeck, D. G., Kokubun, S., and Mukai, T.: Transient flux enhancements in the magnetosheath, Geophys. Res. Lett., 25, 1273–1276, https://doi.org/10.1029/98GL50873, 1998.

Němeček, Z., Šafránková, J., Goncharov, O; Přech, L., Zastenker, GN, Ion scales of quasi-perpendicular low-Mach-number interplanetary shocks Geophys. Res. Lett., 40 (16): 4133–4137, 2013.

Ofman, L., Balikhin, M., Russell, C. T., and Gedalin, M. (2009), Collisionless relaxation of ion distributions downstream of laminar quasi-perpendicular shocks, J. Geophys. Res., 114, A09106, doi:10.1029/2009JA014365.

Ofman, L., and Gedalin, M. (2013), Two-dimensional hybrid simulations of quasi-perpendicular collisionless shock dynamics: Gyrating downstream ion distributions, J. Geophys. Res. Space Physics, 118, 1828– 1836, doi:10.1029/2012JA018188.

642 Omidi, N., D. Sibeck, O. Gutynska, and K. J. Trattner (2014), Magnetosheath filamentary
643 structures formed by ion acceleration at the quasi-parallel bow shock, J. Geophys. Res.
644 Space Physics, 119, 2593–2604, doi:10.1002/2013JA019587.

645 Paschmann, G., and S. J. Schwartz (2000), ISSI Book on Analysis Methods for Multi-
646 Spacecraft Data, in Cluster-II Workshop Multiscale / Multipoint Plasma Measurements,
647 ESA Special Publication, vol. 449, edited by R. A. Harris, p. 99.

648 Palmroth, M., Hietala, H., Plaschke, F., Archer, M., Karlsson, T., Blanco-Cano, X., Sibeck,
649 D., Kajdič, P., Ganse, U., Pfau-Kempf, Y., Battarbee, M., and Turc, L.: Magnetosheath
650 jet properties and evolution as determined by a global hybrid-Vlasov simulation, Ann.
651 Geophys., 36, 1171-1182, https://doi.org/10.5194/angeo-36-1171-2018, 2018.

652 Plaschke, F., H. Hietala, and V. Angelopoulos (2013), Anti-sunward high-speed jets in the
653 subsolar magnetosheath, Ann. Geophys., 31, 1877–1889, doi:10.5194/angeo-31-1877-
654 2013.

655 Plaschke, F., Hietala, H., Archer, M., Blanco-Cano, X., Kajdic, P., Karlsson, T., Lee, S. H.,
656 Omidi, N., Palmroth, M., Royter-shteyn, V., Schmid, D., Sergeev, V., and Sibeck, D.:
657 Jets Downstream of Collisionless Shocks, Space Science Reviews, 214,
658 81,https://doi.org/10.1007/s11214-018-0516-3, 2018.

659 Plaschke, F. and Hietala, H.: Plasma flow patterns in and around magnetosheath jets, Ann.
660 Geophys., 36, 695-703, https://doi.org/10.5194/angeo-36-695-2018, 2018.

661 Pollock, C., T. Moore, A. Jacques, J. Burch, U. Gliese, Y. Saito, T. Omoto, L. Avanov, A.
662 Barrie, V. Coffey, J. Dorelli, D. Gershman, B. Giles, T. Rosnack, C. Salo, S. Yokota, M.
663 Adrian, C. Aoustin, C. Auletti, S. Aung, V. Bigio, N. Cao, M. Chandler, D. Chornay, K.
664 Christian, G. Clark, G. Collinson, T. Corris, A. DeÂăLosÂăSantos, R. Devlin, T. Diaz, T.
665 Dickerson, C. Dickson, A. Diekmann, F. Diggs, C. Duncan, A. Figueroa-Vinas, C.
666 Firman, M. Freeman, N. Galassi, K. Garcia, G. Goodhart, D. Guererro, J. Hageman, J.
667 Hanley, E. Hemminger, M. Holland, M. Hutchins, T. James, W. Jones, S. Kreisler, J.
668 Kujawski, V. Lavu, J. Lobell, E. LeCompte, A. Lukemire, E. MacDonald, A. Mariano, T.
669 Mukai, K. Narayanan, Q. Nguyan, M. Onizuka, W. Paterson, S. Persyn, B. Piepgrass, F.
670 Cheney, A. Rager, T. Raghuram, A. Ramil, L. Reichenthal, H. Rodriguez, J. Rouzaud, A.
671 Rucker, M. Samara, J.-A. Sauvaud, D. Schuster, M. Shappirio, K. Shelton, D. Sher, D.
672 Smith, K. Smith, S. Smith, D. Steinfeld, R. Szymkiewicz, K. Tanimoto, J. Taylor, C.
673 Tucker, K. Tull, A. Uhl, J. Vloet, P. Walpole, S. Weidner, D. White, G. Winkert, P.-S.
674 Yeh, and M. Zeuch (2016), Fast plasma investigation for magnetospheric multiscale,
675 Space Sci. Rev., pp. 1–76, doi:10.1007/s11214-016-0245-4.

676 Russell, C. T., B. J. Anderson, W. Baumjohann, K. R. Bromund, D. Dearborn, D. Fischer, G.
677 Le, H. K. Leinweber, D. Leneman, W. Magnes, J. D. Means, M. B. Moldwin, R.
678 Nakamura, D. Pierce, F. Plaschke, K. M. Rowe, J. A. Slavin, R. J. Strangeway, R.
679 Torbert, C. Hagen, I. Jernej, A. Valavanoglou, and I. Richter (2014), The Magnetospheric
680 Multiscale Magnetometers, Space Sci. Rev., doi:10.1007/s11214-014-0057-3.

681 Savin, S., E. Amata, L. Zelenyi, V. Budaev, G. Consolini, R. Treumann, E. Lucek, J.
682 Safrankova, Z. Nemecek, Y. Khotyaintsev, M. Andre, J. Buechner, H. Alleyne, P. Song,
683 J. Blecki, J.L. Rauch, S. Romanov, S. Klimov, A. Skalsky, High energy jets in the Earth's

magnetosheath: implications for plasma dynamics and anomalous transport. JETP Lett. 87, 593–599 (2008).

Savin, S., E. Amata, L. Zelenyi, V. Lutsenko, J. Safrankova, Z. Nemecek, N. Borodkova, J. Buechner, P.W. Daly, E.A. Kronberg, J. Blecki, J. Budaev, L. Kozak, A. Skalsky, L. Lezhen, Super fast plasma streams as drivers of transient and anomalous magnetospheric dynamics. Ann. Geophys. 30, 1–7 (2012). https://doi.org/10.5194/angeo-30-1-2012

Scholer, M., and Burgess, D. (1992), The role of upstream waves in supercritical quasi-parallel shock re-formation, J. Geophys. Res., 97(A6), 8319– 8326, doi:10.1029/92JA00312.

Schwartz, S.J., Magnetic field structures and related phenomena at quasi-parallel shocks. Adv. Space Res. 11, 231–240 (1991). https://doi.org/10.1016/0273-1177(91)90039-M

Schwartz, S.J., D. Burgess, W.P. Wilkinson, R.L. Kessel, M. Dunlop, H. Luehr, Observations of short large amplitude magnetic structures at a quasi-parallel shock. J. Geophys. Res. 97, 4209–4227 (1992). https://doi.org/10.1029/91JA02581

Shue, J.-H., Song, P., Russell, C. T., Steinberg, J. T., Chao, J. K., Zastenker, G., Vaisberg, O. L., Kokubun, S., Singer, H. J., Detman, T. R., & Kawano, H. (1998). Magnetopause location under extreme solar wind conditions. Journal of Geophysical Research, 103(A8), 17,691–17,700. https://doi.org/10.1029/98JA01103

Soucek, J., Escoubet, C. P., and Grison, B. (2015), Magnetosheath plasma stability and ULF wave occurrence as a function of location in the magnetosheath and upstream bow shock parameters, J. Geophys. Res.-Space, 120, 2838–2850.

Vuorinen, L., Hietala, H., and Plaschke, F.: Jets in the magnetosheath: IMF control of where they occur, Ann. Geophys., 37, 689–697, https://doi.org/10.5194/angeo-37-689-2019, 2019.

Wilson, L. B., Koval, A., Sibeck, D. G., Szabo, A., Cattell, C. A., Kasper, J. C., Maruca, B. A., Pulupa, M., Salem, C. S., and Wilber, M. (2013), Shocklets, SLAMS, and field-aligned ion beams in the terrestrial foreshock, J. Geophys. Res. Space Physics, 118, 957– 966, doi:10.1029/2012JA018186.

Yang, Z. W., Lu, Q. M., Lembège, B., and Wang, S. (2009a), Shock front nonstationarity and ion acceleration in supercritical perpendicular shocks, J. Geophys. Res., 114, A03111, doi:10.1029/2008JA013785.

Yang, Z. W., Lu, Q. M., and Wang, S. (2009b), The evolution of the electric field at a nonstationary perpendicular shock, Phys. Plasmas, 16, 1.

Yang, Z. W., Lembège, B., and Lu, Q. M. (2012), Impact of the rippling of a perpendicular shock front on ion dynamics, J. Geophys. Res., 117, A07222, doi:10.1029/2011JA017211.